REPORT DOCUMENTATION PAGE

AFRL-SR-AR-TR-08-0068

PLEASE DO NOT RETURN YOUR FORM TO THE ABOVE ADDRESS.

1. REPORT DATE *(DD-MM-YYYY)*	2. REPORT TYPE	3. DATES COVERED (From – To)
	Final Technical Report	1 April 2004 – 31 March 2007

4. TITLE AND SUBTITLE
Development of Ceramics with Highly Organized Microstructures

5a. CONTRACT NUMBER

5b. GRANT NUMBER
FA9550-04-1-0185

5c. PROGRAM ELEMENT NUMBER

6. AUTHOR(S)
Dr. Gary Messing

5d. PROJECT NUMBER

5e. TASK NUMBER

5f. WORK UNIT NUMBER

7. PERFORMING ORGANIZATION NAME(S) AND ADDRESS(ES)
Dept of Materials Science & Engineering & Materials Research Institute
Pennsylvania State University
University Park PA 16802

8. PERFORMING ORGANIZATION REPORT NUMBER

9. SPONSORING/MONITORING AGENCY NAME(S) AND ADDRESS(ES)
USAF/AFRL
AFOSR
875 North Randolph Street
Arlington VA 22203
Dr Joan Fuller/NA

10. SPONSOR/MONITOR'S ACRONYM(S)
AFOSR

11. SPONSORING/MONITORING AGENCY REPORT NUMBER
N/A

12. DISTRIBUTION AVAILABILITY STATEMENT

Distribution Statement A: Approved for public release. Distribution is unlimited.

13. SUPPLEMENTARY NOTES

14. ABSTRACT

Enhanced spatial control of microstructure development during sintering allows for access to finely engineered properties in ceramics. Predominately single phase ceramics with highly organized microstructures have been fabricated in two different systems: Al_2O_3 and $BaTiO_3$. In the Al_2O_3 system, samples were processed with a focus on spatial control of microstructure development. Distinct regions of different grain sizes, degree of texture, and single crystal were fabricated in situ within single samples. The size scale (down to ~5 m), morphology, periodicity, and connectivity of these regions were controlled during fabrication using conventional ceramic processing techniques. In the $BaTiO_3$ system, a different approach was taken. Patterned microstructures were obtained using two different photolithographybased techniques. Grain growth enhancing dopants were patterned on the surface and subsequent heat treatments result in periodic regions of randomly oriented large grains. For the other approach, a patterned single crystal was used as local templates for solid state conversion of the polycrystal. In this experiment, significant growth of the single crystal regions (more than 0.5 mm in depth) was achieved in the presence of modest matrix coarsening.

15. SUBJECT TERMS

16. SECURITY CLASSIFICATION OF:	17. LIMITATION OF ABSTRACT	18. NUMBER OF PAGES	19a. NAME OF RESPONSIBLE PERSON
		31	

FINAL TECHNICAL REPORT

Development of Ceramics with Highly Organized Microstructures

Grant No. FA9550-04-1-0185

April 1, 2004 – March 31, 2007

Submitted by:

Gary L. Messing and Susan Trolier-McKinstry
Department of Materials Science and Engineering and Materials Research Institute
Pennsylvania State University
University Park, PA 16802

Abstract:

Enhanced spatial control of microstructure development during sintering allows for access to finely engineered properties in ceramics. Predominately single phase ceramics with highly organized microstructures have been fabricated in two different systems: Al_2O_3 and $BaTiO_3$. In the Al_2O_3 system, samples were processed with a focus on spatial control of microstructure development. Distinct regions of different grain sizes, degree of texture, and single crystal were fabricated *in situ* within single samples. The size scale (down to ~5 μm), morphology, periodicity, and connectivity of these regions were controlled during fabrication using conventional ceramic processing techniques. In the $BaTiO_3$ system, a different approach was taken. Patterned microstructures were obtained using two different photolithography-based techniques. Grain growth enhancing dopants were patterned on the surface and subsequent heat treatments result in periodic regions of randomly oriented large grains. For the other approach, a patterned single crystal was used as local templates for solid state conversion of the polycrystal. In this experiment, significant growth of the single crystal regions (more than 0.5 mm in depth) was achieved in the presence of modest matrix coarsening.

1. Introduction:

The properties of ceramics are governed by a combination of intrinsic crystallographic and extrinsic microstructural characteristics. Traditionally, these properties have been accessed through the use of either single crystals or randomly oriented polycrystals. These constitute the opposite ends of a spectrum on which directional properties occupy one end and averaged isotropic properties lie on the other. In many cases, however, the applicability of such materials is limited. For example, single crystals tend to lack the mechanical integrity of polycrystals and are often expensive and/or time-consuming to produce, while the isotropic nature of randomly oriented polycrystals is simply not well-suited to applications that require property anisotropy or the unique properties of a defined crystallographic direction.

For years, researchers have sought to bridge the ends of the single crystal/random polycrystal spectrum by introducing texture to polycrystals.[1, 2] Texture has been attained in metallic systems by inducing plastic deformation through a variety of high shear techniques such as hot rolling, cold rolling, and wire drawing. These techniques, however, are not applicable to less compliant systems such as brittle ceramics; thus new approaches were needed. A recent innovation in this regard is the introduction of the templated grain growth (TGG) process,[2] whereby a subset of anisotropic particles (e.g. platelets and whiskers) is oriented during green body fabrication. These oriented particles

serve as templates for epitaxial nucleation of textured grains. The preferential growth of the oriented grains into the non-oriented matrix results in a microstructure predominately consisting of similarly oriented grains. Such a microstructure provides access to property anisotropy approaching that of the corresponding single crystal while retaining some of the mechanical integrity of a polycrystal. There are limitations to the quality of texture that can be achieved. Within the casting plane, the template alignment and placement is more random, causing a higher degree of misorientation and distribution of texture in the final compact.

Other methods for texturing ceramics include TGG using magnetic alignment and Assisted Biaxially Textured Substrates (RABiTS). The process to magnetically align templates is limited to materials that are magnetic or strongly crystallographically anisotropic, and anisometric grains. Magnetic template alignment is also limited to producing good template alignment in the magnetic field direction; a more random placement of templates develops in all other directions. This gives rise to comparable alignment quality to that observed with the tape casting TGG method. RABiTS involves a process that produces textured metal substrates used for epitaxial growth of oxides. The orientation, size, and distribution of the textured grains by the RABiTS process are difficult to control. The following Table outlines the FWHM values that have been reported for the degree of orientation for each technique. As show in Table I, there is room for improvement to produce textured materials with lower FWHM values.

Table I: FWHM values for the different processing techniques

Process	FWHM (in Degrees)
Tape Cast TGG	6 – 20[3, 4]
Magnetic Alignment	8 – 12[5]
RABiTS	5 – 10[6, 7]

Besides texture, many ceramic properties are dependent upon other microstructure features such as grain size, intergranular phases, and porosity. In non-cubic systems, for example, primary grain size effects have been identified for properties such as fracture toughness, compressive and tensile strength, hardness, wear resistance, dielectric loss,

optical scattering, and thermal shock resistance.[8] The presence and crystallinity of grain boundary phases can have a pronounced effect on electrical properties,[9] fracture behavior,[10] and corrosion resistance.[11] Porosity especially can have a dominating effect on a wide range of mechanical, electrical, and optical properties. It is clear that the accessible properties can be quite varied within a given material and that control of microstructure development is crucial for the attainment of the desired property set.

Unique sets of properties can be accessed in composites that are not necessarily intrinsic to either constituent by tailoring the connectivity.[12] Connectivity is defined as the number of dimensions in which each composite component is self-connected. In dual component composites for example, a 3-3 composite is one in which both components are interpenetrating and fully connected in three dimension, while a 2-2 composite is one in which both composites are only connected in two dimensions, i.e. a laminate. The dependence of properties on connectivity is especially pronounced in active properties (i.e. electrical, magnetic, optical, etc). The classic example given by Newnham *et al.* is that of a composite consisting of two non-pyroelectric phases.[12] When combined in an appropriate fashion, the composite exhibits pyroelectricity. In addition to accessing unique properties, the existing properties can be enhanced. Perhaps the most common application is the 1-3 piezoelectric composite transducer, which is used in medical ultrasound imaging, sensors, transmitters, and underwater acoustics. As opposed to the piezoelectric component alone, the composite can be tailored to combine a high thickness mode electro-mechanical coupling factor with low acoustic impedance, small mechanical quality factor, and a reasonably high composite dielectric constant. Passive (i.e. mechanical) properties can also be greatly enhanced by combining different mechanical properties in specific composite designs. Structural composites have been made utilizing combinations of materials with high wear resistance and flaw tolerance, high fracture

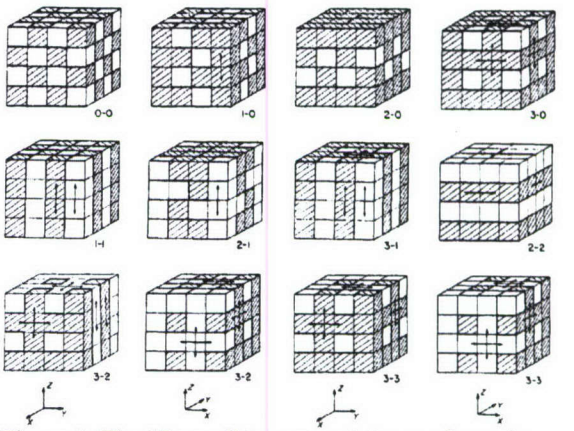

Figure 1. The 12 possible connectivity configurations for dual component composites.

toughness and low density, high and low modulus, etc. The combinations are nearly endless and as such composites have been engineered to better suit a great deal of structural applications.

Composite fabrication can present some challenges and limitations. In some cases the composite components are fabricated independently and combined *ex situ*. This becomes increasingly challenging as components become increasingly small and complex. In other cases, the constituents are fabricated *in situ* with limited spatial or crystallographic control. *In situ* fabrication presents significant hurdles related to both thermal expansion mismatch and chemical stability. Thermal expansion mismatch can result in significant residual stresses, which can lead to cracking or phase separation. It is necessary that the individual components be chemically compatible to avoid diffusion gradients and new phase nucleation at the component interface. It is clear that traditional composites present limitations on the range of materials and properties that can be accessed.

2. Research Goal and Objectives:

The overall goal of this research project was to develop processes to produce ceramics with highly organized microstructures with controlled spatial distribution, different connectivities, and orientation. This goal was attempted by two significantly different approaches for the $BaTiO_3$ an Al_2O_3 material systems, each with specific objectives.

The objective of the patterned grain growth in $BaTiO_3$ direction was two fold; 1) develop a process that would enable the control of texture in a polycrystalline matrix with vastly improved spatial, orientation, and alignment control and 2) improve the piezoelectric properties of $BaTiO_3$ with increasing texture development. By designing and controlling the template features (size, shape, etc.) and their placement, we can control the amount of textured growth to produce perfectly oriented grains.

The objective of the microstructural composites in Al_2O_3 direction was to demonstrate the range of microstructure combinations, possible connectivities, and their resulting properties. This work focused mainly on 2-2 composite connectivity with the property characterizations focused largely on mechanical properties.

Patterned Grain Growth in $BaTiO_3$:

3. Results:

The first objective, which includes the fabrication of a small grained polycrystalline $BaTiO_3$ matrix and a technique for forming the template size and placement on a single crystal substrate, is the foundation for achieving the remaining research objectives. The two aspects of this objective are outlined below.

3.1 $BaTiO_3$ polycrystalline matrix:

The thermodynamic driving force for template growth during TGG is inversely proportional to the average matrix grain size. Thus it is important to produce a dense polycrystalline matrix with the smallest grain size possible. The fabrication technique used to produce the $BaTiO_3$ matrix with the required characteristics was tape casting.

The as-received $BaTiO_3$ powder (Sakai Chem., MBT-02) was mixed with ethanol and xylenes in a 50/50 ratio with 3.5wt% blown menhaden fish oil (MFO) and ball milled for 24hrs. Afterwards 2.8wt% poly(vinyl) butanol (PVB), 1.3wt% of polyethanlene glycol (PEG) and butylbenzyl phthalate were each added to the suspension and ball milled for an additional 24hrs. The slurry was then de-aired prior to tape casting.

Tapes were cast at 200 μm with a speed of 30 cm/min. The dried tape was cut into 10 cm^2 samples, stacked and uniaxially laminated at 70°C for 5 - 10 minutes and then isostatically laminated at 70°C and 200 MPa for 30 minutes. Sample thicknesses after lamination were approximately 1.0 – 1.5 mm. The samples were then heated to 650°C for 2hrs in air to remove the organics. The samples were isostatically pressed to 175 MPa prior to sintering.

Sintering was conducted either in air or in a reducing furnace. The samples were heated to 1300°C at 5°C/min and cooled at the same rate. The samples fired in the reducing furnace were sintered in a $PO_2 \sim 10^{-11}$ atmosphere. The densities of the sintered samples were measured by Archimedes method and the average grain size was measured either by the linear intercept method[13] or by fracture surface analysis.

Figure 2 shows the average grain size as a function of relative density. The black line follows the typical curve for the sintering $BaTiO_3$ in air, while the red line indicates

the samples fired in the reducing environment. Figure 2 illustrates that as the density approaches 100% of theoretical density, the grain size dramatically increases for the samples fired in air. The samples fired in air between 1300°C to 1350°C produced an average grain size that is too large for any subsequent bonding and growth runs.

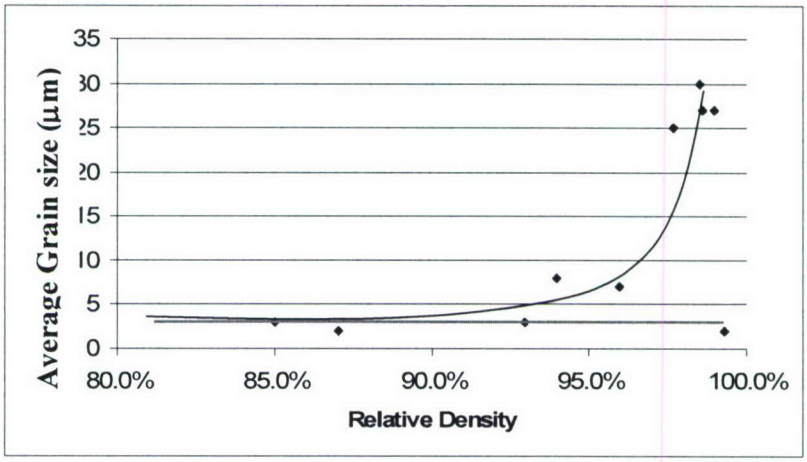

Figure 2: Average grain size as a function of relative density for normal sintering (black line) and reducing sintering at PO_2 $1x10^{-11}$ atm (red line).

Thus a different sintering approach was necessary to reduce the average grain size. Previous studies have shown that for sintering in low PO_2 ($<10^{-15}$ atm), grain boundary motion is retarded.[14] Using this concept, a dense (>99%TD) compact was fabricated with an average grain size of 4 microns (Figure 3).

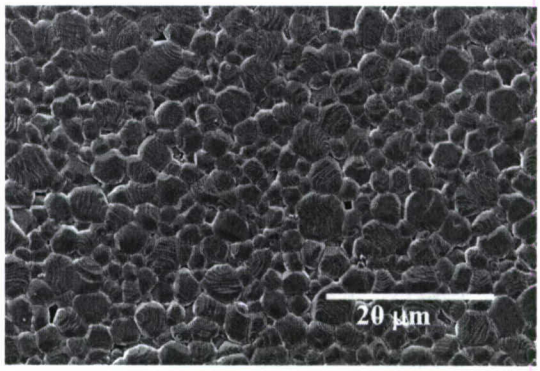

Figure 3: SEM image showing the polished and etched surface of the $BaTiO_3$ sample fired in PO_2 $1x10^{-11}$ atm at 1300°C for 1.5hrs.

3.2 Template formation:

Templates for this study were generated using an optical photolithography process. $BaTiO_3$ single crystal surfaces were patterned to obtain a range of 'template' sizes, shapes, and spacings.

For template formation the single crystal substrate was cleaned prior to sputter coating a 100 nm thick nickel seed layer on the polished surface. A positive photoresist (AZ 1827) was spin coated on the nickel seed layer at 4000 rpm for 40 seconds to produce a photoresist layer of 3 microns. The pattern was soft-baked by heating to 100°C for 1 min, exposed to UV light for 6 seconds through the mask, and developed for 40 seconds (CD-26). Nickel was then electroplated onto the exposed nickel seed layer for 0.5 hours to produce a final nickel thickness of 3 microns. The photoresist was removed and the single crystal substrate was etched via ICP-RIE for 8 hour. This produced a 3micron template relief. Figure 4 shows the etched single crystal with an array of square templates. Any remaining nickel was removed with a combination of HNO_3 and HCl in a 3:1 ratio respectively.

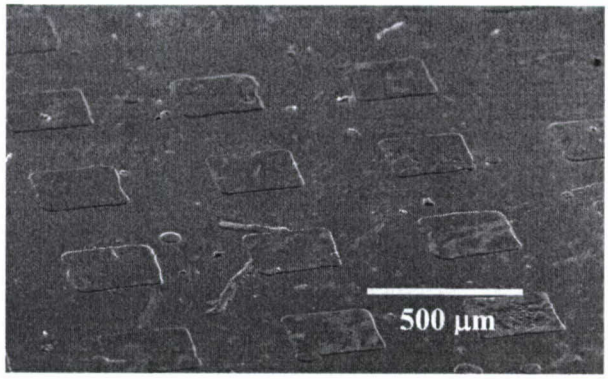

Figure 4: SEM image of the etched single crystal showing the raised templated areas.

The second objective was to understand the conditions for sustained texture growth without significant matrix coarsening to produce a pillar structure with discrete single crystals. The conditions that had an effect on the texture growth were; 1) single crystal orientation, 2) chemistry / dopant level, 3) atmosphere conditions, and 4) defect chemistry in $BaTiO_3$.

3.3 TiO_2 interface layer and matrix coarsening:

In Figure 2, the samples that were fired in air show a larger average grain size then the samples fired in the reducing environment. This concept was applied to the growth runs in order to control the matrix coarsening, since sintering $BaTiO_3$ in a reducing environment limits the presence of abnormal grain growth and limits the coarsening behavior.[14] A study on the matrix coarsening and the effect of the TiO_2 layer on the microstructure was conducted using the growth conditions of 1300°C at a PO_2 of $1x10^{-5}$ atm.

An experiment to test the viability of using TiO_2 or SiO_2 as an interfacial layer was conducted. Two sets of samples were prepared, one with a 25 nm TiO_2 layer and the other with a 25 nm SiO_2 layer. The samples were fired without using a single crystal, and both samples showed local grain enhancement. The experiment was repeated using a [100] $BaTiO_3$ single crystal. With a TiO_2 interfacial layer, the single crystal bonded to the polycrystalline $BaTiO_3$, and the single crystal boundary propagated into the matrix. With the SiO_2 interfacial layer, the single crystal bonded to the matrix, however the single crystal boundary did not propagate into the matrix. XRD analysis on the SiO_2

sample showed the formation of $Ba_2TiSi_2O_8$, which inhibited motion of the single crystal boundary. Thus TiO_2 was chosen as an interfacial layer to promote the formation of a local liquid phase at the boundary aiding in bonding of the single crystal templates and propagation of the single crystal boundary.

TiO_2 layers of 50nm, 100nm, and 150nm thick were spin coated on polished $BaTiO_3$ polycrystalline samples. Photolithography was used to produce a pattern of 1000 μm lines separated by 1000 μm spacing for each TiO_2 thickness. Each set of samples was fired to 1300°C in PO_2 of $1x10^{-5}$ atm for 0.5, 1, or 2hrs. The cross sections were polished and thermally etched, and the microstructure was analyzed. Figure 5 shows the effect of a 50nm or 150nm TiO_2 layer on the grain size and microstructure located directly underneath the TiO_2 layer after sintering for an hour at 1300°C.

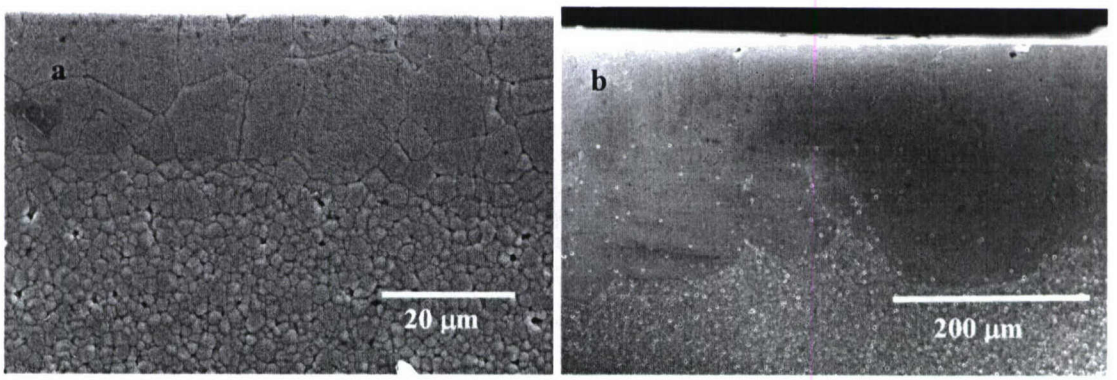

Figure 5: SEM images indicating the enhanced growth from a) 50nm and b) 150nm TiO_2 from the surface for samples fired to 1300°C

The TiO_2 deposited on the surface of the $BaTiO_3$ matrix enhanced the grain growth as indicated in the upper portions of the cross sectioned samples in Figure 6. This is consistent with prior reports on samples that are Ti – rich.[15, 16] The depth of grain growth enhancement was dependent on the amount of TiO_2 deposited, as illustrated in Figure 5. The depth of grain growth enhancement was plotted for each TiO_2 layer thickness as a function of dwell time at 1300°C and is shown in Figure 6.

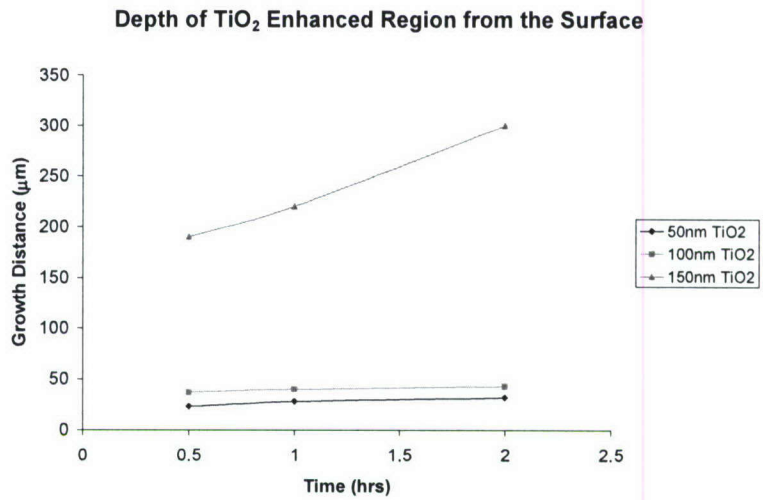

Figure 6: Plot indicating the relative effect of the 50, 100, 150nm TiO_2 on the depth of grain enhancement.

Figure 6 shows that as the dwell time increases, the depth of TiO_2 enhancement of the grain growth also increases. It is interesting to note that the 150nm TiO_2 sample produced a significantly larger growth distance than the other samples. Figure 7 shows the microstructure of the remaining matrix material after 2hrs at 1300°C and a PO_2 of $1x10^{-5}$ atm. When TiO_2 was used as an interfacial bonding layer, the TiO_2 layer was minimized to prevent significant matrix coarsening (and thus a reduction in the driving force) to occur before the single crystal boundary has propagated into the matrix. Using a 0.25M TiO_2 solution, a 25nm thick TiO_2 bonding layer was produced by spinning at 4000 rpm for 30 seconds. In Figure 7, the remaining microstructure still had an average grain size of 4 μm, indicating that little matrix coarsening occurred. Earlier studies showed that grain growth suppression occurred between $1x10^{-11}$ to $1x10^{-18}$ atm and grain growth occurs in higher PO_2 ranges. However, in this work, no significant grain growth was observed for the samples heated in $1x10^{-5}$ atm.[14]

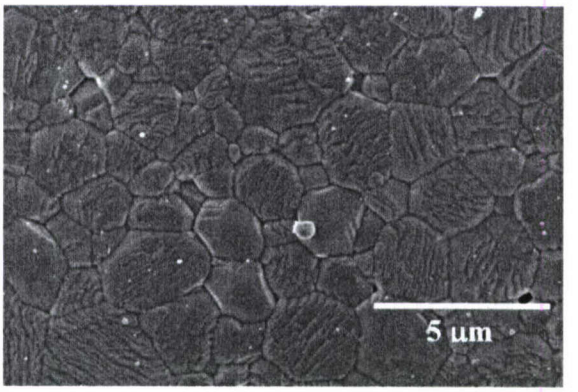

Figure 7: SEM image of the remaining matrix after 2hrs at 1300°C in PO_2 $1x10^{-5}$ atm.

3.4 Bonding/ interface chemistry:

Additional experiments were used to determine an appropriate method for bonding a single crystal $BaTiO_3$ to the polycrystalline matrix. The bonding experiments were conducted with an unetched $BaTiO_3$ single crystal and a polycrystalline $BaTiO_3$ matrix at 1350°C for 2hrs in air. Contact was maintained between the materials by the application of a 40 gram mass placed on top of the single crystal. Two sets of experiments were conducted both with and without a 25nm TiO_2 interface layer.

Figure 8 shows the examples of bonding a [100] $BaTiO_3$ single crystal to the matrix material (a) with and (b) without a 25nm TiO_2 layer. The samples were heated to 1350°C in air and showed a more successful bonding (more area bonded and converted) for the case with a TiO_2 interface layer. This suggested that the interfacial layer between the two materials aided in the contact of the materials at the interface and promoted a more intimate contact for bonding and textured growth. However, in previous work by Rehrig et al.,[17] bonding and growth of the single crystal was accomplished without an interfacial layer and with no applied load. The main difference was Ba/Ti ratio of the starting $BaTiO_3$ matrix. In the Rehrig work the Ba/Ti ratio was 0.95, while the ratio was 0.996 for this study. The addition of a TiO_2 interface layer thus apparently compensated for the less Ti-rich matrix. By keeping the Ba/Ti ratio higher, control over the matrix coarsening was possible while achieving a mobile single crystal interface.

Growth in air at 1350°C yielded significant matrix coarsening, with a grain size approaching 50 – 100 µm. This destroyed the driving force for crystal conversion and drastically limited the single crystal growth.

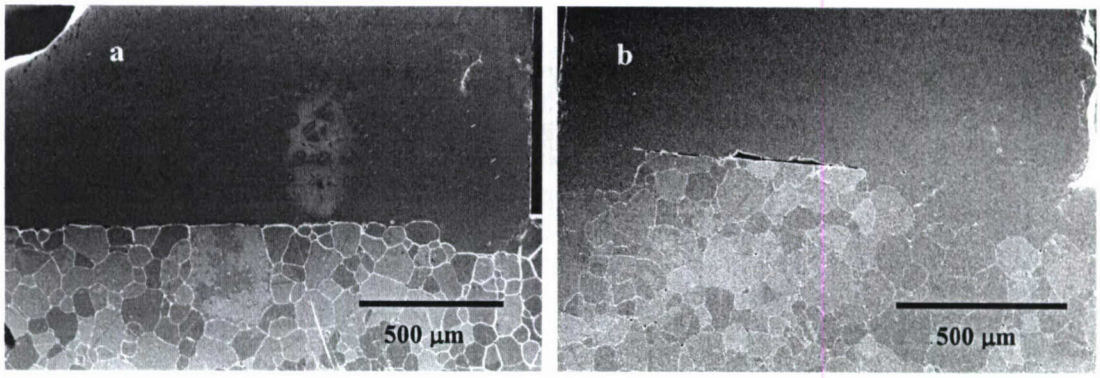

Figure 8 SEM images of single crystal bonding and growth for samples fired in air at 1350°C for 2hrs (a) without and (b) with a TiO_2 interface layer.

The same bonding experiment that was conducted in air was repeated using a PO_2 of $1x10^{-5}$ atm, and a 25nm thick TiO_2 interface layer was used. Figure 9 shows a dark field optical image of a [100] $BaTiO_3$ single crystal bonded to the polycrystalline matrix, with the inset image being an SEM micrograph of the remaining matrix material. The sample was heated to 1300°C in PO_2 of $1x10^{-5}$ atm for 9 hours. The single crystal was grown to a depth of 600 microns (~65 μm/hr); with complete bonding across the entire face of the $BaTiO_3$ single crystal. The SEM inset micrograph shows the remaining matrix material after the 9 hr dwell. The matrix material has an average grain size of 6 μm, which was significantly smaller than the samples fired in air.

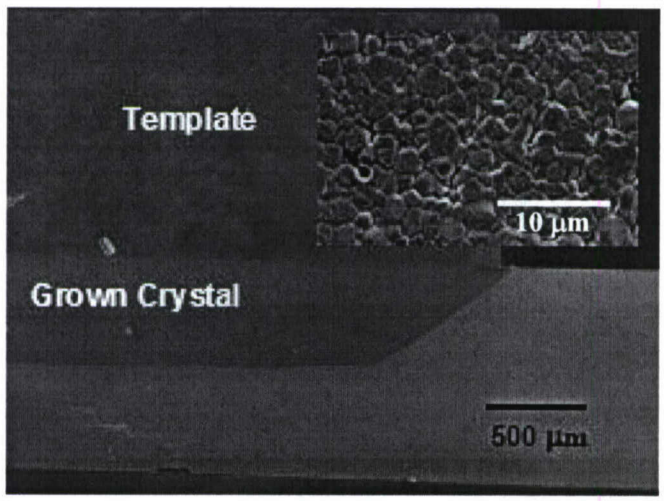

Figure 9: Optical image of converted crystal from a [100] $BaTiO_3$ single crystal with the inset SEM image of the remaining matrix material.

3.5 Patterned textured growth in $BaTiO_3$:

Texture development and growth rates for single crystal patterned templates were conducted using [100] and [110] $BaTiO_3$ single crystals patterned and etched in a line pattern with each template being 1000 μm in width with 1000 μm spacing. The length of each line pattern was 3 – 4 mm. The pattern was chosen to study the vertical and lateral growth rates for each template orientation to understand the kinetics involved with textured growth. After the bonding and growth runs (ranging from 0.5 – 2 hrs), a cross section of each sample was cut, polished and thermally etched. The combination of optical images in Figure 10 shows a [110] patterned single crystal bonded to the matrix material. The figure shows "before" and "after" images from a 3hr growth run that illustrated the texture growth.

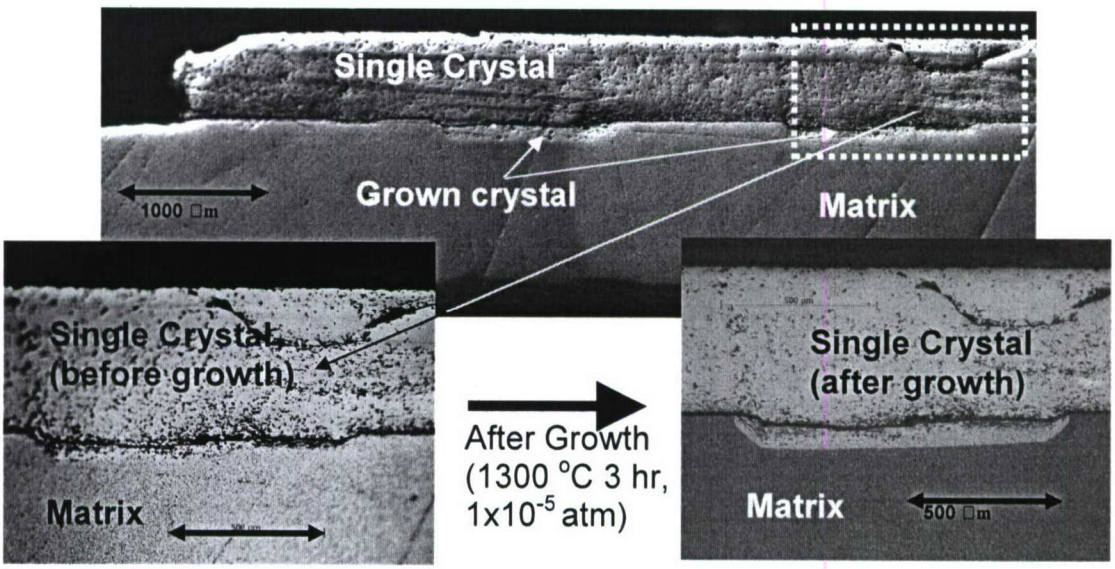

Figure 10: Optical images showing the patterned (100) $BaTiO_3$ crystal before and after a 3hr growth run.

Initial results indicated that the vertical growth rates were on the order of 10 – 15 μm/hr, while the lateral growth rates were more dependent on the orientation of the single crystal (10 – 15 μm/hr for (100) and 5 – 10 μm/hr for (110)). However, in Figure 11, the lateral growth rates were drastically changed when the distance between the templates decreased. In the figure, the initial spacing between the templates was 250 μm. After 3 hr. at 1300°C, the gap between the individual templates was converted to single crystal, which indicated lateral growth rates of 80μm/hr.

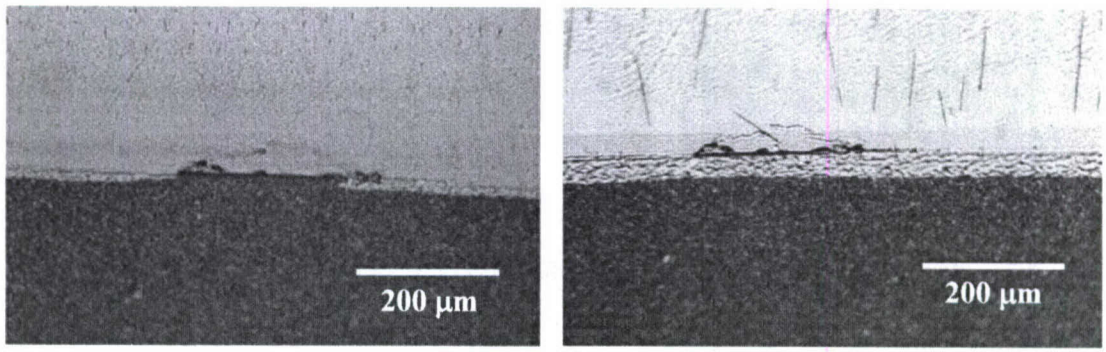

Figure 11: Optical images showing before (a) and after (b) a 3hr growth at 1300°C indicated lateral growth rates of 80μm/hr, which was faster than the 5 – 10 μm/hr previously observed.

4. Conclusion and Future Work:

A process was determined for producing patterned texture in polycrystalline $BaTiO_3$. A technique for fabricating 99%TD polycrystalline $BaTiO_3$ with an average grain size of 4 μm (used as the matrix for texture growth) was accomplished. Optical lithography and dry etching was used to produce templates of controlled size, shape, and periodicity. Growth conditions such as temperature, atmosphere, etc. were optimized for the patterned grain growth experiments. Initial growth rates for the [100] and [110] $BaTiO_3$ single crystal orientation for the vertical and lateral directions were determined to range between 5 – 15 μm/hr.

Additional experiments can be conducted with smaller template sizes (<1000 μm), with template spacings increasing from 50 – 400 microns to ascertain the template spacing limit for which the textured growth rates are increased. Also experiments on the [100] and [110] patterned crystals in different oxygen atmospheres should be conducted to determine if there is an effect of the PO_2 level on textured growth.

Measurements of the dielectric and piezoelectric properties as a function of increasing texture fraction would enable the understanding of how the dielectric constant, hysteresis, piezoelectric coefficients, etc. are affected as a function of periodic texture volume.

Microstructural Composites in Al_2O_3:

5. Introduction:

Three general types of microstructure composites have been developed to demonstrate the utility and range of the microstructure composite concept. The first type is the grain size composite, wherein the primary difference in microstructure is grain size. This is achieved by local control of boundary mobility during grain growth. The second type is textured-equiaxed composites. These are composed of textured sections and equiaxed components. In addition to local boundary migration control, templated grain growth (TGG) processes were used to yield textured microstructures. The third type is single crystal-equiaxed composites. These are composed of equiaxed ceramic with sections of single crystal selectively grown by the solid state conversion process.

Spatial control and connectivity of individual features in a microstructure composite are ultimately the key to developing useful and unique properties. Microstructural features can be controlled via the starting location and transport of the dopants, minority second phases, and liquid phases that are used to manipulate microstructure development. The initial location of these species is set during processing. Tape casting is a processing technique that is particularly well-suited for the fabrication of composites with 2-2 connectivity (sometimes referred to as laminates). This approach is appropriate as the chemistry of the tapes is controlled during slurry formulation and tapes with distinct chemistries can be stacked. With tapes as thin as 5 μm, the starting location of microstructure development controlling species can be finely tuned.

6. Al_2O_3 as a Model System:

It was important to choose a model system that has a) a wealth of understanding and literature with regards to microstructure development from which to draw and b) useful and sufficiently anisotropic property sets that warrant further exploitation. The most extensively studied ceramic, particularly with respect to microstructure development, is α-Al_2O_3 (alumina). Information has been published concerning diffusion coefficients, rate-controlling mechanisms, growth morphology and kinetics, dopant effects, etc. This knowledge provided a suitable base where methods for spatial control

of microstructure was developed. Alumina has shown to be a highly useful material, owing to its thermal, mechanical, optical, and chemical resistance properties.

6.1 Dopant and Second Phase Effects:

To fully demonstrate the capabilities of the microstructure composite concept, it was important to produce composites with well-defined sections of distinct microstructure features. This was accomplished by maintaining microstructure development on a local level during the heat treatments by crystalline grain boundary second phases (ZrO_2, Al_2TiO_5), boundary mobility-enhancing dopants (TiO_2), intergranular liquid phases (SiO_2), and dopants that controlled the solid solubility of liquid formers (MgO). A very brief summary of the relevant effects of each of these species on microstructure development will be presented. They will be discussed further in context as they are used to produce various microstructure composites.

Second phase particles (such as ZrO_2, Al_2TiO_5) retard grain growth though a particle drag mechanism.[18] The particles reduced the mobility and effectively pin boundaries. This was because the movement of a grain boundary with a second phase particle required either particle-boundary separation (which carries a free energy penalty associated with the creation of additional grain boundary area) or the physical drag of the particle. Alumina didn't generally have a high enough boundary mobility to induce particle boundary separation and thus the boundary was pinned.

TiO_2 has been used as a sintering aid in alumina[19, 20] and it is known to enhance grain growth once the dopant concentration exceeds a threshold concentration (between 0.05 and 0.2 cation percent).[21] This grain growth enhancement was not a result of a change in diffusivity, but in boundary mobility. For example, the mobility in undoped alumina at 1350°C was reported as 9.8×10^{-18} $m^4 J^{-1} s^{-1}$.[22] The mobility of 0.4 wt% TiO_2-doped alumina was reported as 1.3×10^{-17} $m^4 J^{-1} s^{-1}$, an increase of almost 33%. Other studies reported a far greater increase in mobility, up to 2 orders of magnitude.[21] While the literature presents conflicting results, it appears that TiO_2 does not form an intergranular phase in high purity alumina and acts as a solid state dopant.

The presence of intergranular liquid phases, and especially silicates, has long been known to increase grain growth and abnormal grain growth rates.[23, 24] The transport

processes that so often limit grain growth in the solid state are increased greatly by changing the mechanism from grain boundary diffusion to solution-precipitation. In part because of the enhanced kinetics, grains can grow more readily towards their equilibrium shapes. In anisotropic systems, this means that the presence of liquid phases commonly results in anisotropic grain growth. In the alumina system, this results in grains with platelet-like morphologies.[24]

MgO has a large number of effects on microstructure development in alumina.[25] Most importantly for our purposes, however, was that MgO has shown to increase the solid solubility of silicon ions in alumina, thus eliminating the appearance of a liquid phase at low SiO_2 concentrations.[26, 27] At the same time the solid solubility of MgO is increased as well. This phenomenon was a result of the creation of a neutral and strain compensating defect complex between substitutional magnesium and silicon ions that has a greatly decreased boundary interaction potential. We took advantage of this increased co-solubility in order to locally engineer the appearance of a liquid phase to attain the desired microstructural features.

7. Results:

7.1. 2-2 Textured-Equiaxed Composites

The two components in textured-equiaxed microstructure composites are crystallographically textured polycrystal and randomly oriented equiaxed polycrystal. Textured-equiaxed composites are of particular interest because of their potentially interesting mechanical properties. Textured materials have shown to have enhanced fracture toughness, though commonly at the expense of strength. Therefore it may be possible to combine these heightened fracture toughness and intrinsic high strength characteristics in a single phase composite.

Texture was developed in this study via the templated grain growth (TGG) process. The original work demonstrating TGG was performed on alumina by Seabaugh *et al.*[2] It was shown that by orienting anisotropic template particles (e.g. particles that serve as nucleation sites for grain growth) during processing and sintering with liquid phase additives excellent density and a high degree of texture can be achieved. Since that time, others have textured alumina but the lessons remain the same. Platelet loading a)

should be below 20 wt% to achieve dense samples; and b) ultimately determines the size of the grains in fully textured materials. The platelets should be sufficiently large so as to have a thermodynamic growth advantage over the powder. Most importantly, a liquid phase was necessary for several reasons. The main reason was that it relieves the stresses associated with constrained sintering around large template particles. The secondary reasons were it enhanced the kinetics of template growth and promotes growth anisotropy in the alumina system.[24]

In textured-equiaxed composites, equiaxed ceramic were in contact with textured ceramic. Unfortunately the rapid propagation of liquid phase via grain boundary wetting away from the textured layers made retaining equiaxed grains near this interface an issue. Therefore we have developed a strategy of locally controlling the solid solubility of liquid forming species (SiO_2) through the use of dopants (MgO). Figure 12 shows the critical concentrations of each species required for abnormal grain growth.[26] Concentration ranges used for the two layers are also shown in Figure 12. We were able to confine the appearance of liquid phase to the textured component by doping the equiaxed component with MgO. SiO_2 that diffuses into the equiaxed component was brought into solid solution. Therefore, within this section, there was no liquid phase and microstructure development occurred via solid state diffusional processes. Within the textured region, microstructure development occurred via a solution-precipitation mechanism.

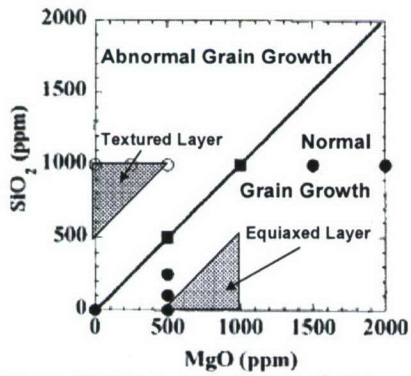

Figure 12. Grain growth map plotting the type of growth according to the silica and magnesia concentrations. Gavrilov *et al* (2003). *JMatSci* 38, 3965-72.[16]

7.1.1. Processing

Tapes intended for texturing included 10 wt% alumina platelets, which were oriented under the doctor blade during casting. Enhanced growth of the templated grains in the textured layers was accomplished by 500-1000 ppm SiO_2 as a liquid former. 1000 ppm MgO was incorporated into the adjacent layers to prevent the onset of abnormal grain growth due to silica diffusion. However, because an undetermined amount of MgO

from the adjacent layers diffused into the intergranular liquid (and thus its exact composition is unknown), the temperature required for the appearance of the liquid phase was determined experimentally. Figure 13 shows SEM micrographs after sintering at three different temperatures. At 1400°C, there was some growth of the templated particles; however from the amount of growth and the lack of grain faceting, it was clear that there was no liquid phase. At 1600°C, while there was sufficient template growth, abnormal grain growth was rampant in the equiaxed section (the middle of the image). At 1500°C, while there was sufficient liquid phase to accomplish TGG, the adjacent areas were still fine-grained and relatively equiaxed. Further investigation showed that conditions for local TGG are appropriate at 1450-1550°C for the chemistry used here.

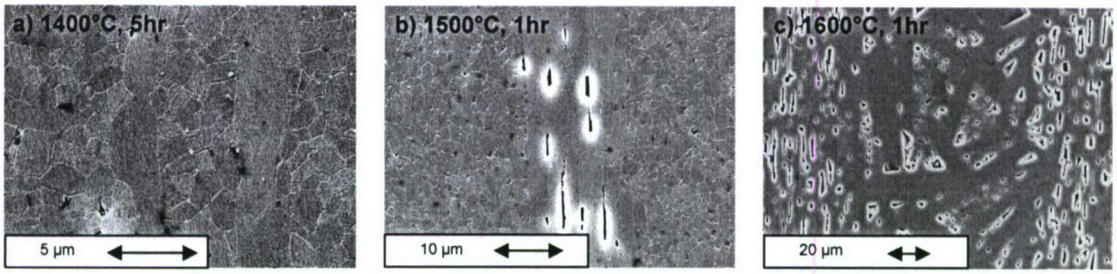

Figure 13. SEM images of 2-2 textured-equiaxed composites with various sintering temperatures. Notes: a) Within the textured layer; b) single textured layer; c) the left and right hand sides are the textured layers and the center is a formerly equiaxed layer that has been overrun with abnormal grain growth.

Figure 14 shows higher magnification SEM micrographs of the textured-equiaxed interface. Figure 14a shows that the textured grains were fairly well-aligned. Texture analysis was not performed. It is evident from Figure 14b that the textured and equiaxed sections were well–bonded and the interface largely takes on the morphology of the basal surface of the templated grain (i.e., flat). However, it appeared that the equiaxed section actually contains some faceted grains with small but non-unity aspect ratios. This implied that a liquid phase was, in fact, present to some degree in the equiaxed sections. It is not clear as to whether the difference in grain growth between the sections was due to a difference in kinetics or simply a result of larger starting grains (templates).

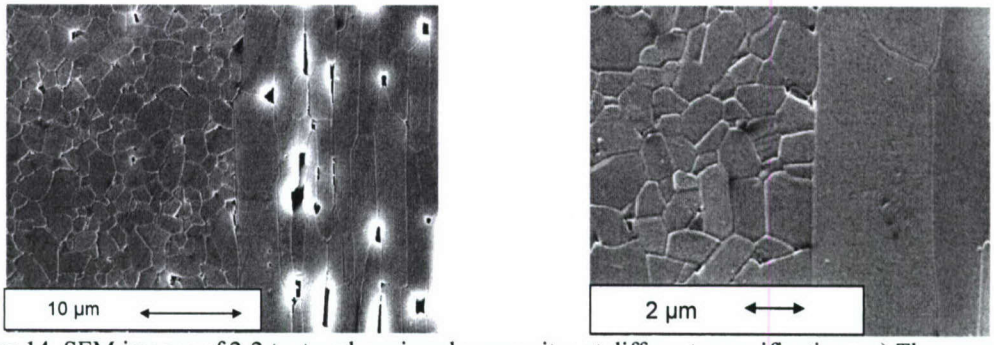

Figure 14. SEM images of 2-2 textured-equiaxed composites at different magnifications. a) There was no effect of the silica on the equiaxed region; b) There was a straight interface between the equiaxed grains and the basal surface of the textured grain. Also, there was no excess porosity at this interface.

7.1.2 Fracture Behavior:

Analysis of the fracture behavior of 2-2 textured-equiaxed composites was performed. First, indentation was used to determine the effect of texture on crack length. A typical result produced is shown if Figure 15a. The relative crack lengths are shown for cracks into and parallel to the textured layers. A similar sample was fractured (by hand) normal to the layers to examine the fracture path and determine if the textured layers had an effect. The fracture path was greatly affected by the presence of textured layers. Crack deflection occurred within most of the textured layers and extends at least 50 µm normal to the fracture direction. In Figure 15b, a fracture surface was shown indicating the different crack paths. The image was taken slightly off-normal to the main fracture surface (sections B and C) so that the deflection path (section A) was seen. It is evident from this image that crack propagation was transgranular *through* the textured layer and intragranular *along* the textured layer during deflection (between basal surfaces of platelet grains).

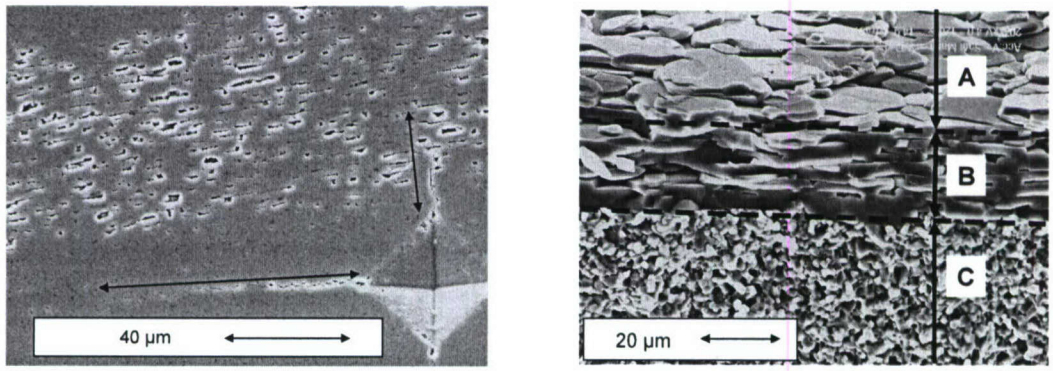

Figure 15. SEM images of 2-2 textured-equiaxed composite. a) Relative crack lengths induced by Vicker's

indentation parallel to and into the textured layer; b) Fracture surface slightly off-normal to sections B and C. The crack deflects into the page between section A and B.

Single edge notched beam (SENB) fracture measurements were performed using a 4-point bend geometry. The sample geometry was 45mm x 4mm x 3mm, with a notch depth of 0.5h. No deliberate pre-cracking was performed, though it was assumed that the notch cutting produced sufficiently sharp pre-cracks. The test was performed on several identical samples with varying crosshead speeds. Results are shown in Figure 16. Figure 6a shows the force-displacement curve for 3 of the trials. Every measurement shows extensive crack deflection. The crack deflection in one sample was correlated to the crack that caused it (Figure 16b). The crack extends laterally in both directions (off the image) a total of nearly 10 mm before continuing through the remainder of the sample. This deflection (and all others observed) occurred within the textured layers and not between layers. Another words, this result was not a consequence of poor inter-layer adhesion (or processing) but of the weak adhesion between basal surfaces of textured grains.

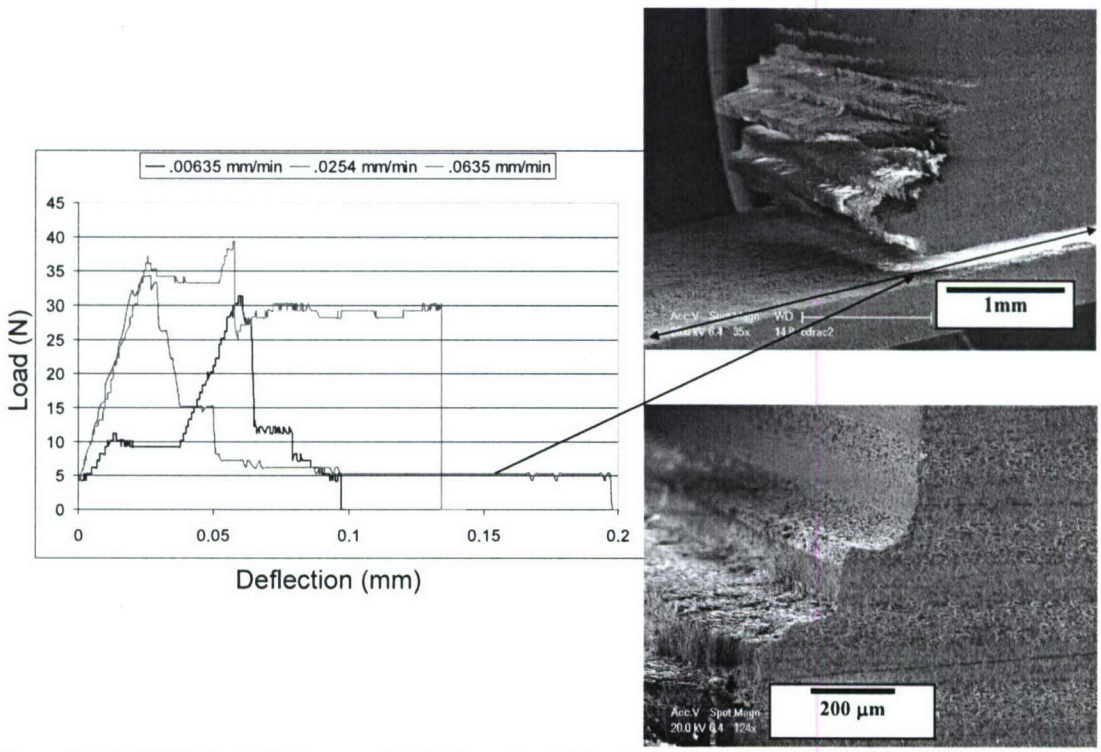

Figure 16. a) SENB load-displacement data from 4-point bend test. The different curves correspond to different cross-head speeds. The extensive displacement in the (0.0254mm/min) sample was correlated to an extremely large deflection in both directions (b) prior to completion of failure through the remaining four layers.

7.2. 2-2 Grain Size Composites:

The two components in grain size composites are randomly oriented polycrystals. The distinction between the components was that of grain size, and in some cases grain morphology. The attainment of such microstructural differences was accompanied by fewer restrictions than in the previous section where a liquid phase was necessary. Grain growth in random ceramics was affected by a wide variety of species. We chose to explore two different strategies utilizing different methods of microstructure control.

The first strategy was to use ZrO_2 second phase particles to inhibit grain growth in one component and allow grain growth in the other component to proceed unhindered. This produced a grain size difference that was a function of the amount of ZrO_2 inclusions. The second strategy employed TiO_2 in excess of the solubility limit. This resulted in the nucleation and growth of Al_2TiO_5 second phase particles that inhibited grain growth in that volume. The Ti-rich regions acted as a source of TiO_2, which enhanced grain growth in the adjacent areas. Because there is a diffusion gradient of TiO_2 away from the source component, it was possible to incorporate grain size gradients into these structures.

The following should be noted concerning control of grain growth via TiO_2 or ZrO_2: abnormal grain growth occurred in alumina when an intergranular liquid phase was present. This composition was commonly an aluminosilicate and appeared even in ostensibly 'pure' alumina due to silica impurity. Therefore when isolating the effects of TiO_2 or ZrO_2 additions, it was imperative that the unintentional consequences of impurity silica be mitigated. As a result, all grain size composites produced by the utilization of TiO_2 or ZrO_2 are uniformly doped with 500 ppm MgO unless otherwise noted.

7.2.1 Processing

Two different strategies were explored to produce 2-2 grain size composites. The first strategy employed ZrO_2 second phase particles to inhibit grain growth through boundary pinning. ZrO_2 (5 vol% and 10 vol%) was added to the tape cast slurries prior to milling. These tapes were stacked in an alternating sequence with ZrO_2-free tapes. SEM images of the samples with different ZrO_2 content was sintered at 1471°C and 1550°C

and shown in Figure 17. The images are centered on the boundary between the different grain size regions. The brighter contrast phase is ZrO_2.

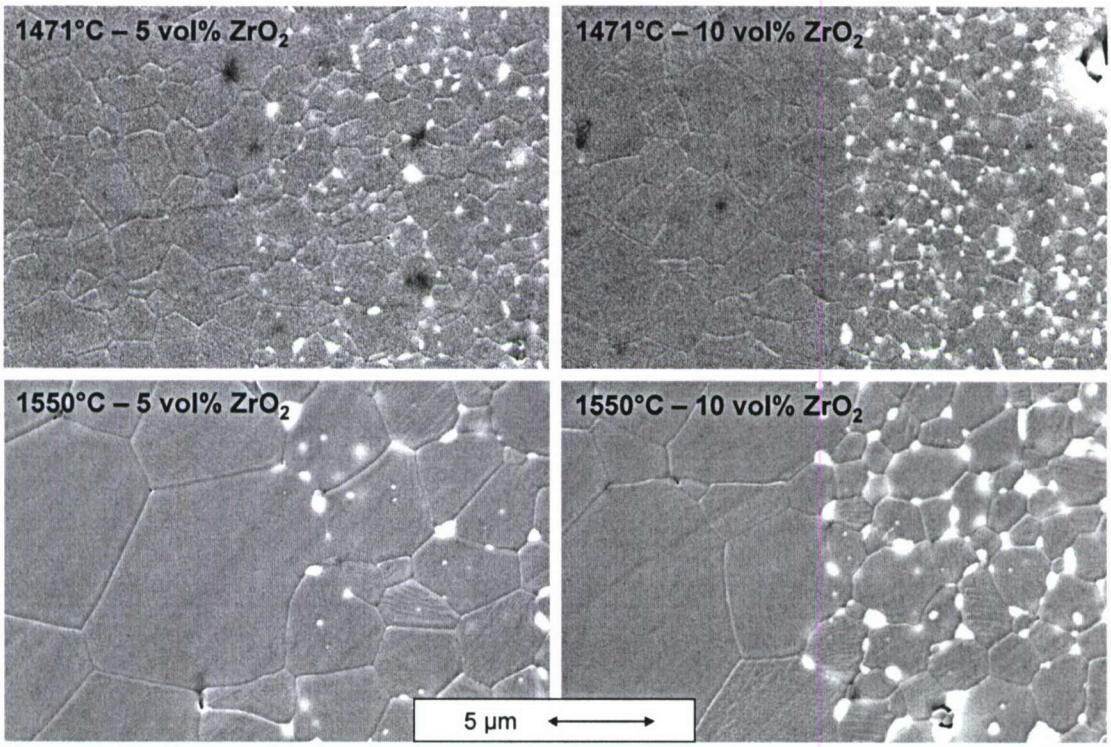

Figure 17. SEM images of the interface between microstructures in grain size composites using ZrO_2 to locally inhibit grain growth.

In all cases the interface between the different grain size regions was quite sharp. There was no nucleation of ZrO_2 particles outside of the intended region. As expected, the only evolution of the ZrO_2 particles during heat treatment was coarsening. This suggested that this method was applicable to the production of microstructure composites with very thin layers, approaching the order of the final grain size. Also as expected, an increase in vol% ZrO_2 resulted in increasingly effective grain growth inhibition. This resulted in the ability to produce a greater transition in grain size across the boundary.

The second strategy employed TiO_2 in excess of the solubility limit (10 wt%). In the 'source' layers with the excess TiO_2, the nucleated second phase Al_2TiO_5 particles inhibited grain growth by pinning grain boundaries, while the TiO_2 enhanced grain growth in the adjacent layers. This means that, in comparison to the zirconia strategy, a greater transition in grain size was achieved for the same vol% of second phase. The effect of TiO_2 on grain growth was a function of its concentration. Therefore because

there was a diffusional gradient of TiO_2 away from the source layer there was also greater freedom in tailoring microstructure gradients into these composites. Figure 18 shows SEM micrographs of select results.

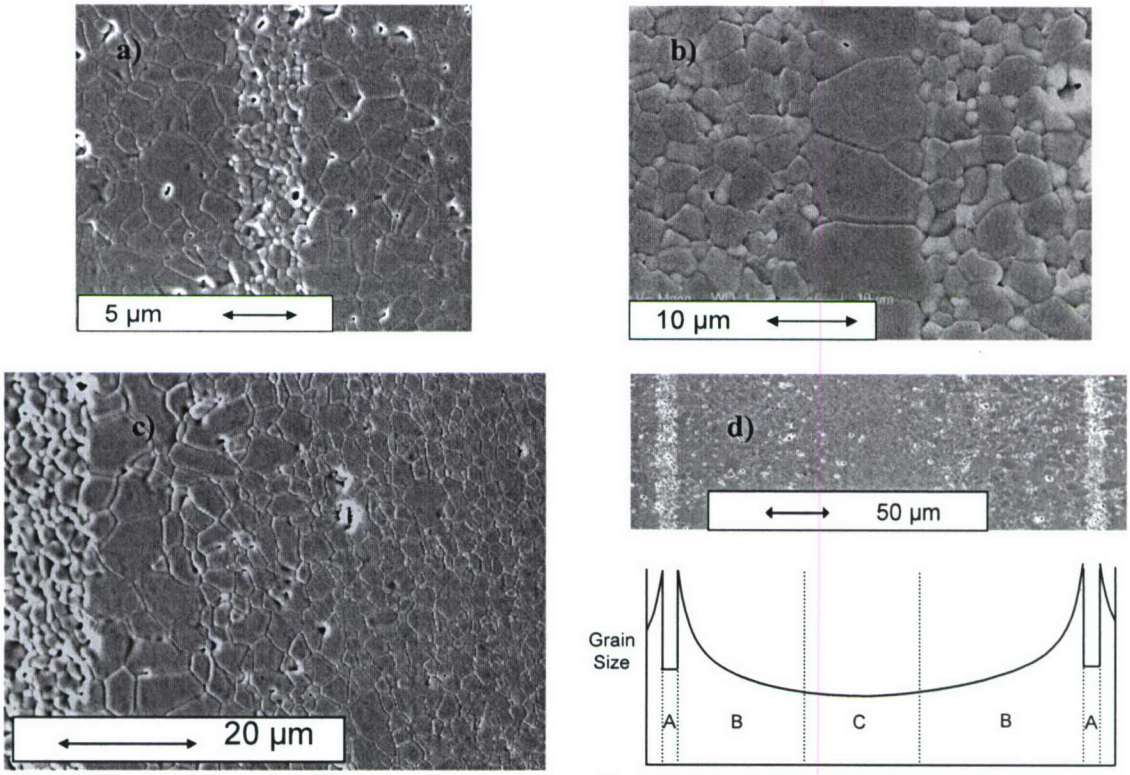

Figure 18. SEM images of various microstructure composites utilizing Al_2TiO_5-TiO_2 for microstructure control. a) Al_2O_3-(10 vol%)Al_2TiO_5 thin layer surrounded by alumina with TiO_2 grain growth enhancement; b) Single grain width thin layer surrounded Al_2O_3-(10 vol%)Al_2TiO_5 ceramic; c) Al_2O_3-(10 vol%)Al_2TiO_5 thin layer next to a graded microstructure (due to TiO_2 gradient); d) graded grain size composite (similar to c) with corresponding schematic grain size profile

In Figure 18a, the thin layer in the middle was the TiO_2 source layer. Note the ~5 μm layer thickness achieved by tape casting. The thermal conditions were set such that the enhanced region is relatively homogeneous. The exact reasons that these thermal conditions resulted in a homogenous (i.e. not graded) microstructure were unclear and are in need of further examination. In Figure 18b, the thick layer was the TiO_2 source layer. In this case, the thin nature (and consequent short diffusion distance) of the adjacent layer assured a homogenous microstructure. In fact, in much of the sample the thin layer was a single grain thick. Graded microstructures are shown in Figures 18c and 18d. The gradient in grain size was finely controlled by temperature and dopant concentration at the source. In Figures 18c and 18d the gradient was smooth. This wasn't always the case.

Figure 19 shows the microstructure of a sample that was surface-doped with a TiO_2 sol-gel coating. It was clear that the grain size transition was quite sharp, approaching step-like. This type of transition has not yet been achieved in composite samples, partially due to the difficulty in correlating surface layer thickness to in-body dopant concentration. Figure 17d portrays the versatility of this strategy and the range of microstructures that it can produce. The grain size profile of a graded grain size 2-2 composite was plotted schematically. There are three sections. Section A was the source layer, section B was the part of the adjacent layer that was affected by TiO_2 diffusion, and section C was the unaffected zone of the adjacent layer. Aspects of this profile that can be directly (and semi-independently) controlled included the thickness of each section, the magnitude of the grain size in each section, and the severity of the gradation in section B. These were controlled by tape thicknesses, dopant concentrations, and characteristics of the thermal treatment.

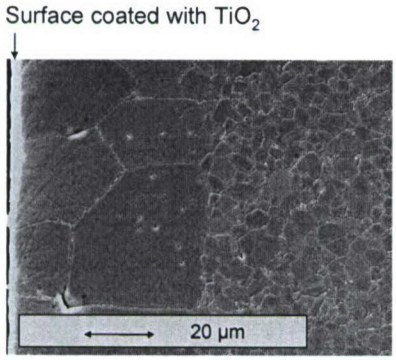

Figure 19. Cross-section SEM image near the surface of an alumina sample with a TiO_2 sol-gel surface coating.

7.3. 2-2 Single Crystal-Equiaxed Composites:

Single crystal-equiaxed composites are of interest for a number of reasons. For any active directional properties, these would outperform their textured-equiaxed composite counterparts. More importantly if high quality crystals were grown between thin polycrystalline layers it would produce what would be considered a textured ceramic with unprecedented texture quality. The single crystal component of 2-2 single crystal-equiaxed composites was produced by the solid state conversion (SSC) process. In SSC, a single grain migrates through the sample and converts the rest of the ceramic (or matrix) into a single crystal.[28, 29] The original grain can be within the ceramic but was more commonly seeded from another single crystal. As with grain growth, the driving force for this process was the reduction of grain boundary free energy. Therefore conversion was maximized when small matrix grain size was retained.

We used both TiO_2 and SiO_2 to selectively promote SSC. Ceramic samples were prepared in a similar manner as previous sections. Samples were pre-sintered at 1300-1400°C for 15 minutes to obtain near full density in order to avoid constrained sintering at the bond interface. The samples were then cut normal to the layer plane with a slow speed diamond saw, polished to a 6 μm finish, and bonded to a-plane sapphire. A schematic of this process is shown in Figure 20.

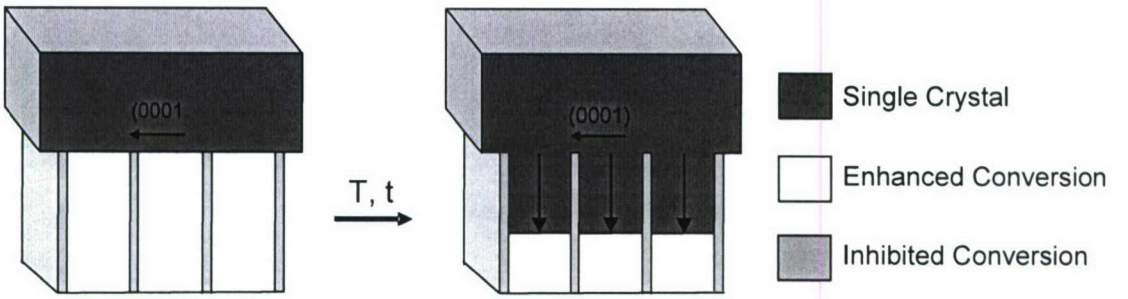

Figure 20. Schematic of the production of 2-2 single crystal-equiaxed composites.

Producing 2-2 single crystal-equiaxed composites was challenging and the results are mixed. Some results are shown in Figure 21. Figure 21a shows a composite that used Al_2TiO_5 (~10 vol%) to prevent SCC and TiO_2 to enhance SCC. The single crystal was grown approximately 40-50 μm. The inset image shows the front edge of the Al_2O_3-Al_2TiO_5 section, outlined by its original position. It resisted conversion and maintained its morphology quite well during the conversion of the other section. Figure 21b shows the results using SiO_2 to enhance SCC and MgO to inhibit SCC (by reducing the effect of the SiO_2). While the conversion was more extensive and sustainable (e.g. the matrix grain size is still small), the morphology of the conversion regions was not maintained. We hypothesized a two part approach to solve this problem. The first is to prevent nucleation at the front edge of the equiaxed sections. One way this can be accomplished is to change the polishing characteristics. We have found that the difference in grain boundary chemistry caused the polishing rates to be different. This can be exploited to create a gap between the original crystal and the equiaxed section. The second part is to orient the single crystal such that the basal plane lies in-plane with the layers. This is the slow growth direction and would greatly reduce conversion laterally into the equiaxed section.

While higher quality single crystal-equiaxed composites were produced using TiO_2, future direction could focus solely on using SiO_2-MgO. The reason is that with TiO_2 the dopant is constantly diffusing into the component intended for conversion. Therefore the unconverted matrix is being supplied with ever-increasing TiO_2. This depletes the conversion driving force at an increasing rate during conversion. In the latter system however, all of the SiO_2 is already in the component intended for conversion. If anything it is slowly diffusing out of this component. Sustained conversion in this case should rely upon finding the processing and firing conditions to achieve conversion while avoiding abnormal growth in the matrix. This is how SSC is commonly performed.

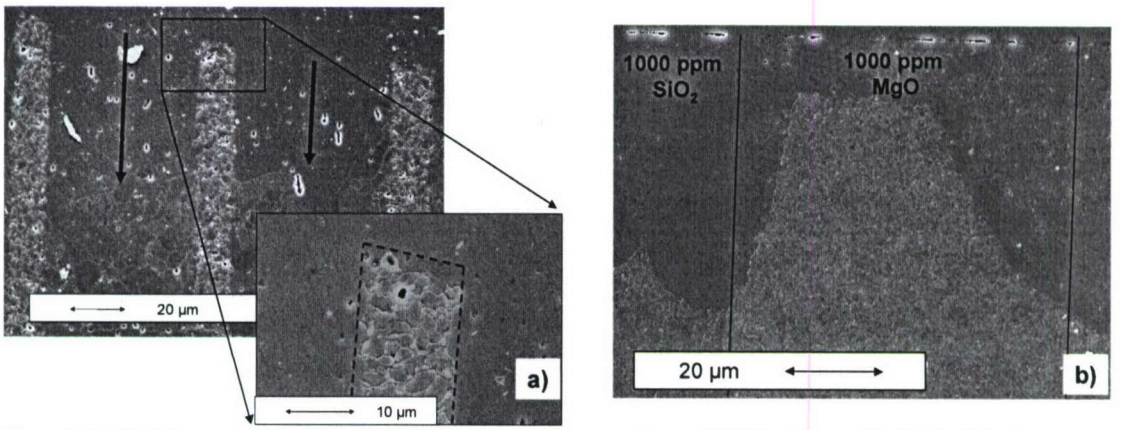

Figure 21. SEM images of 2-2 single crystal-equiaxed composites. a) SSC enhanced by TiO_2. The inset image is a higher magnification image Al_2O_3 with aluminum titanate that remains unconverted; b) SSC enhanced by SiO_2 and limited by MgO.

8. Conclusions:

Precise spatial control of microstructure development using second phases, liquid phases and dopants has been explored in the alumina system. Using these principles, examples of three different types of microstructure composites were successfully fabricated. The types of microstructure composites were grain size composites, textured-equiaxed composites, and single crystal-equiaxed composites. All have 2-2 connectivity and are fully or predominately single phase. Preliminary mechanical properties tests were performed on textured-equiaxed composites. Early results showed promising fracture behavior including evidence of graceful failure with extensive displacements during four-point bend tests.

9. References:

1. Messing, G.L., S. Trolier-McKinstry, E.M. Sabolsky, C. Duran, S. Kwon, B. Brahmaroutu, P. Park, H. Yilmaz, P.W. Rehrig, K.B. Eitel, E. Suvaci, M. Seabaugh, and K.S. Oh, "Templated Grain Growth of Textured Piezoelectric Ceramics," *Critical Reviews in Solid State and Materials Sciences*. **29** 45-96 (2004).

2. Seabaugh, M.M., I.H. Kerscht, and G.L. Messing, "Texture Development by Templated Grain Growth in Liquid-Phase-Sintered Alpha-Alumina," *J. Am. Ceram. Soc.* **80**(5) 1181-88 (1997).

3. Pham-Thi, M., H. Hemery, and H. Dammak, "X ray Investigation of High Oriented (1-x)$PbMg_{1/3}Nb_{2/3}O_3$-(x)$PBTiO_3$ Ceramics," *J. Euro. Ceram. Soc.* **25**(12) 2433-2435 (2005).

4. Yilmaz, H., G.L. Messing, and S. Trolier-McKinstry, "(Reactive) Templated Grain Growth of Textured Sodium Bismuth Titanate ($Na_{1/2}Bi_{1/2}TiO_3$-$BaTiO_3$) Ceramics - I Processing," *J. Electroceramics*. **11** 207-15 (2003).

5. Lewis, J.A., A.C. Read, and T.K. Holmstrom, "Transport Properties of Magnetic Field/Liquid Assisted Textured $YBa_2Cu_3O_{7-x}$ Tape-Cast Films," *IEEE Transactions on Applied Superconductivity*. **7**(2) 1440 - 1443 (1997).

6. Cantoni, C., A. Goyal, U. Schoop, X. Li, M.W. Rupich, C. Thieme, A.A. Gapud, T. Kodenkandath, T. Aytug, M. Paranthaman, K. Kim, J.D. Budai, and D.K. Christen, "Investigation of TiN Seed Layers for RABiTS Architectures with a Single-Crystal-Like Out-of-Plane Texture," *IEEE Transactions on Applied Superconductivity*. **15**(2) 2981-2985 (2005).

7. Norton, D.P., A. Goyal, J.D. Budai, D.K. Christen, D.M. Kroeger, E.D. Specht, Q. He, B. Saffian, M. Paranthaman, C.E. Klabunde, D.F. Lee, B.C. Sales, and F.A. List, "Epitaxial $YBa_2Cu_3O_7$ on Biaxially Textured Nickel (001): An Approach to Superconducting Tapes with High Critical Current Density," *Science*. **274**(5288) 755-757 (1996).

8. Rice, R., *Mechanical Properties of Ceramics and Composites - Grain and Particle Effects*. 2000, NY: Marcel Dekker Inc.

9. Yan, M.F., "Microstructural Control in the Processing of Electronic Ceramics," *Mater. Sci. Eng.* **48** 53-72 (1981).

10. Padture, N.P. and H.M. Chan, "Improved Flaw Tolerance in Alumina Containing 1 vol% Anorthite via Crystallization of the Intergranular Phase," *J. Am. Ceram. Soc.* **75**(7) 1870-5 (1992).

11. Mikeska, K.R., "Corrosion of Alumina in HF," *J. Am. Ceram. Soc.* **83**(5) 1160-4 (2000).

12. Newnham, R.E., D.P. Skinner, and L.E. Cross, "Connectivity and Piezoelectric - Pyroelectric Composites," *Mater. Res. Bull.* **13** 525-36 (1978).

13. Fullman, R.L., "Measurement of Particle Sizes in Opaque Bodies," *J. Metals.* **3** 447-52 (1953).

14. Jung, Y.-I., S.-Y. Choi, and S.-J.L. Kang, "Effect of Oxygen Partial Pressure on Grain Boundary Structure and Grain Growth Behavior in $BaTiO_3$," *Acta. Mater.* **54**(10) 2849-55 (2006).

15. Hennings, D.F.K., R. Janssen, and P.J.L. Reynen, "Control of Liquid-Phase-Enhanced Discontinuous Grain-Growth in Barium Titanate," *J. Am. Ceram. Soc.* **70**(1) 23-27 (1987).

16. Yoo, Y.S., M.K. Kang, J.H. Han, H. Kim, and D.Y. Kim, "Fabrication of $BaTiO_3$ Single Crystals by Using Exaggerated Grain Growth Method," *J. Euro. Ceram. Soc.* **17**(14) 1725-7 (1997).

17. Rehrig, P.W., G.L. Messing, and S. Trolier-McKinstry, "Templated Grain Growth of Barium Titanate Single Crystals," *J. Am. Ceram. Soc.* **83**(11) 2654-60 (2000).

18. Rahaman, M.N., *Ceramic Processing and Sintering.* 1995, NY: Marcel Dekker Inc.

19. Bagley, R., I.B. Culter, and D.L. Johnson, "Effect of TiO_2 on Initial Sintering of Al_2O_3," *J. Am. Ceram. Soc.* **53**(5) 136 (1970).

20. Cahoon, H. and C. Christenson, "Sintering and Grain Growth of Alpha - Alumina," *J. Am. Ceram. Soc.* **39**(10) 337-44 (1956).

21. Horn, D.S. and G.L. Messing, "Anisotropic Grain Growth in TiO_2-doped Alumina," *Mater. Sci. Eng.* **A195** 169-78 (1995).

22. Powers, J.D. and A.M. Glaeser, *Titanium Effects on Sintering Grain Boundary Mobility of Alumina.* Sintering Technology, ed. R.M. German, G.L. Messing, and R.G. Cornwall. 1996: Marcel Dekker Inc., USA. 33-40.

23. Bae, S.I. and S. Baik, "Determination of Critical Concentrations of Silica and/or Calcia for Abnormal Grain Growth in Alumina," *J. Am. Ceram. Soc.* **76**(4) 1065-7 (1993).

24. Kaysser, W.A., M. Sprissler, C.A. Handwerker, and J.E. Blendell, "Effect of Liquid Phase on Morphology of Grain Growth in Alumina," *J. Am. Ceram. Soc.* **70**(5) 339-43 (1987).

25. Bennison, S.J. and M.P. Harmer, *A History of the Role of MgO in the Sintering of* α-Al_2O_3. Sintering of Advance Ceramics, ed. C.A. Handwerker, J.E. Blendell, and W.A. Kaysser. Vol. 7. 1990, Westerville, OH: American Ceramic Society. 13-49.

26. Gavrilov, K.L., S.J. Bennison, K.R. Mikeska, J.M. Chabala, and R. Levi-Setti, "Silica and Magnesia Dopant Distributions in Alumina by High-Resolution Scanning Secondary Ion Mass Spectrometry," *J. Am. Ceram. Soc.* **82**(4) 1001-9 (1999).

27. Handwerker, C.A., P.A. Morris, and R.L. Coble, "Effects of Chemical Inhomogeneities on Grain Growth in Alumina," *J. Am. Ceram. Soc.* **72**(1) 339-43 (1989).

28. Greskovich, C. and J. Brewer, "Grain-Boundary Migration and High Velocity in Al_2O_3," *J. Am. Ceram. Soc.* **90**(5) 1375-81 (2007).

29. Scott, C., M. Kaliszewski, C. Greskovich, and L. Levinson, "Conversion of Polycrystalline Al_2O_3 into Single-Crystal Sapphire by Abnormal Grain Growth," *J. Am. Ceram. Soc.* **85**(5) 1275-80 (2002).